Morphodynamics of barchan and transverse dunes using a cellular automaton model

D. Zhang,[1] C. Narteau,[1] and O. Rozier[2]

Received 4 December 2009; revised 15 April 2010; accepted 12 May 2010; published 29 September 2010.

[1] We analyze the morphodynamics of bedforms produced under unidirectional flow conditions by a lattice gas cellular automaton designed to study sediment transport. In this model, the same instability is responsible for the formation of dunes on flat sand beds and the initiation of superimposed bedforms on dune slopes. In transverse dune fields, secondary bedforms increase crestline sinuosity and number of defects (end of crestlines). On the other hand, avalanches and lateral grain motions tend to eliminate these defects to produce more regular crestlines. Lateral fluxes of sediment are also essential for stabilizing the shape of isolated barchan dunes. We measure the propagation speed of superimposed bedforms on steady state barchan dunes and show how they contribute to the formation and detachment of smaller barchans along horns. The model predicts that barchan dunes are not scale invariant and that their shape varies with respect to the strength of the flow. In addition, we show that the increase in bed shear stress between the ground and the crest is proportional to the dune aspect ratio. Finally, we present a general methodology for estimating the sediment flux over the brink from dune aspect ratio and flow velocity. Using these fluxes, we rescale the propagation speed of different generations of bedforms to verify that dunes and secondary bedforms are dynamically identical. Despite more fluctuations than in the case of isolated barchan dunes, all these geometric and dynamical relationships hold for a population of dunes with complex dune-dune interactions.

Citation: Zhang, D., C. Narteau, and O. Rozier (2010), Morphodynamics of barchan and transverse dunes using a cellular automaton model, *J. Geophys. Res.*, *115*, F03041, doi:10.1029/2009JF001620.

1. Introduction

[2] Dune fields are continuously shaped by a variety of factors, including flow strength and direction, sediment availability, topography and vegetation [*McKee*, 1979; *Breed and Grow*, 1979; *Lancaster*, 1995; *Bristow et al.*, 2000; *Wiggs*, 2001; *Ewing et al.*, 2006; *Baas and Nield*, 2007; *Durán and Herrmann*, 2006]. In addition, smaller dunes are faster and, within dune fields, collisions are frequent and may result in the formation of larger structures by amalgamation or nucleation of secondary bedforms [*Lancaster*, 1992; *Kocurek and Ewing*, 2005; *Elbelrhiti et al.*, 2005]. Such a pattern coarsening is eventually stopped as the flow depth provides an upper limit to dune size [*Andreotti et al.*, 2009]. Simultaneously, other mechanisms of size regulation are likely to result from complex dune-dune interactions during collisions [*Hersen and Douady*, 2005] or specific wind conditions that amplify dune calving [*Elbelrhiti et al.*, 2005]. These mechanisms may also explain why corridors of barchan dunes with a constant dune-size distribution over tens of kilometers are commonly observed [*Hersen et al.*, 2004]. In all cases, populations of crescentic dunes show linear relations between height, length and width [*Finkel*, 1959; *Hastenrath*, 1967, 1987; *Elbelrhiti et al.*, 2008] and various levels of complexity due to the presence of superimposed bedforms. Then, even under unidirectional flow conditions, there are considerable variations in dune morphodynamics (Figure 1). A major challenge is now to model and predict these complex features as well as the constraints imposed at smaller length scale by local field measurements, laboratory experiments and theory.

[3] During the last decades, dune field patterns have been examined through different numerical methods, including sets of partial differential equations [*Sauermann et al.*, 2001; *Kroy et al.*, 2002; *Andreotti et al.*, 2002; *Fischer et al.*, 2008] and cellular automaton (CA) models [*Nishimori and Ouchi*, 1993; *Werner and Gillespie*, 1993; *Werner*, 1995; *Nishimori et al.*, 1999; *Momiji and Warren*, 2000]. Continuous models are based on two major equations, one for the conservation of mass, one for the relation between the sediment flux and the elevation profile (e.g., slope, curvature). These equations may rely on various types of flux saturation mechanisms but, in a vast majority of cases, the flow separation

[1]Laboratoire de Dynamique des Fluides Géologiques, Institut de Physique du Globe de Paris, UMR 7154, CNRS, Université Paris 7, Paris, France.
[2]Service Informatique, Institut de Physique du Globe de Paris UMR 7154, CNRS, Université Paris 7, Paris, France.

Copyright 2010 by the American Geophysical Union.
0148-0227/10/2009JF001620

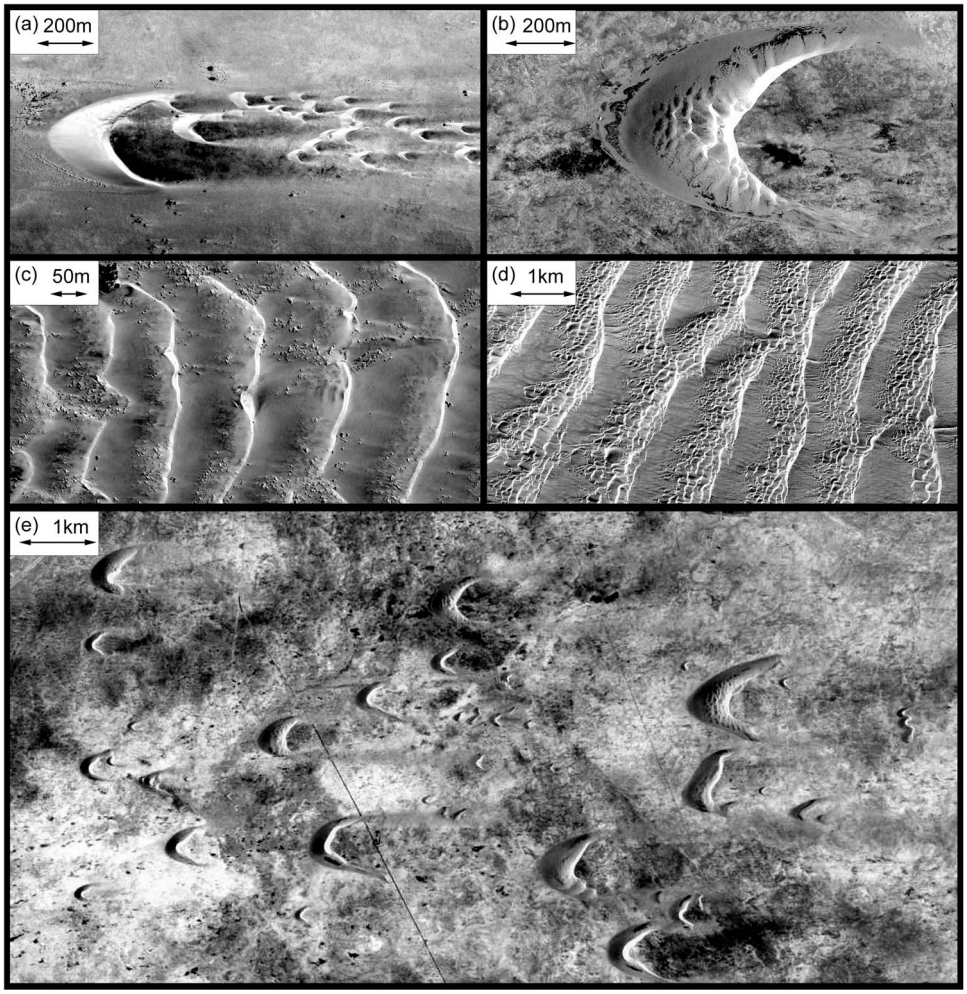

Figure 1. Dune patterns under unidirectional flows. (a) Barchan dunes in Morocco (21°46′12.83″N, 16°39′19.97″W). (b) Superimposed bedforms on a barchan dune in Qatar (24°59′43.20″N, 51°22′18.63″E). (c) Transverse dunes in Angola (16°04′19.15″S, 12°05′58.98″E). (d) Superimposed bedforms on transverse dunes in Namibia (25°51′20.30″S, 14°57′15.25″E). (e) A population of barchan dunes in Qatar (24°59′05.54″N, 51°21′04.16″E). We observed superimposed bedforms at a variety of scales, from an elementary size, on the order of 20 m, perceivable as the typical dimension of the smallest dunes.

and the recirculation eddy in the dune lee are not properly resolved. Instead, there is an envelope function or a separation streamline connecting the brink with a reattachment point. As a result, these models can hardly handle superimposed bedforms and complex flow structures. Moreover, computing power limits the size of the dune fields that can be investigated.

[4] The CA approach recently became a standard for the modeling of morphogenesis and the dynamics of complex systems [*Chopard and Droz*, 1998]. This has been especially true in the physics of sediment transport where CAs have shown to be particularly efficient to reproduce almost all types of dune patterns as well as the role of defects/terminations in the evolution of dune fields [*Werner and Kocurek*, 1997]. Most of these discrete models consider instantaneous motions of the so-called "sand slabs" to mimic sediment transport. Nevertheless, the description of the flow is not precise enough to take into account changes in flow strength and the impact of sediment motions on the transport capacity. In addition, as for all CAs, some arbitrary length scales are involved in the modeling process (e.g., the elementary length scale of the CA, the saltation length of sand slabs). These are major limitations for the quantification of dune field properties when dealing with real situations.

[5] In order to bridge the gap between precise continuous approaches and functional CA models, *Narteau et al.* [2009] proposed a 3-D dune model that combines a CA model for sediment transport and a lattice gas CA for hydrodynamics (section 2). In such an hybrid model, they observed the emergence of a dynamic equilibrium between flow and topography and set the length and timescales of the model from observations. This model can now be used for the modeling and quantification of complex dune field patterns. In this paper, we start this work by presenting bedforms produced under unidirectional flow (barchan dunes in section 3, transverse dunes in section 4). Special attention is given to the origin and role of superimposed bedforms. Thus, we analyze transport and hydrodynamic properties from a limited number of well-defined physical quantities (e.g., flow speed, bed shear stress) to demonstrate that all the

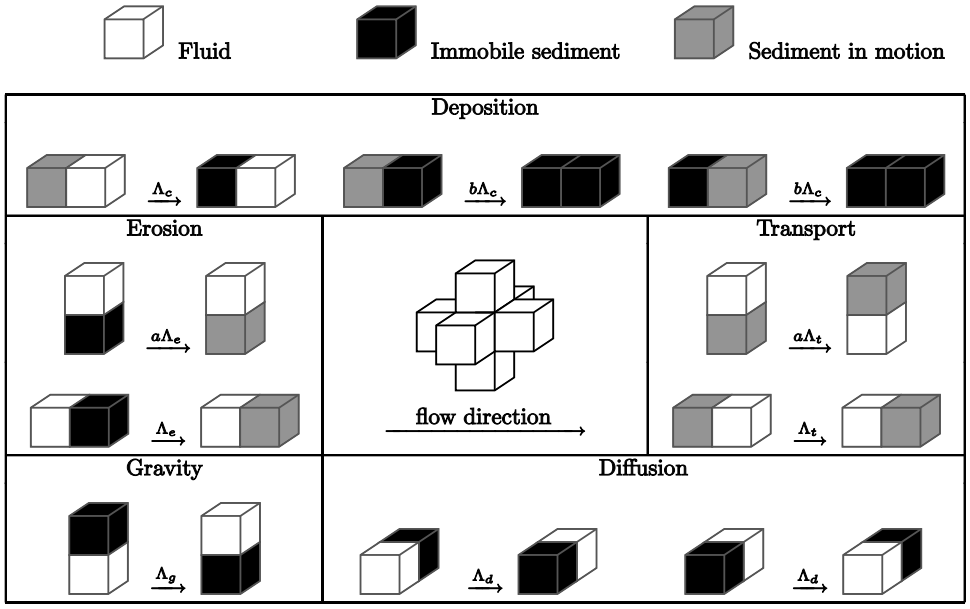

Figure 2. Active transitions of doublets in the cellular automaton model for sediment transport. Different sets of transition are associated with deposition, erosion, transport, gravity, and diffusion. Transition rates with units of frequency are Λ_c, Λ_e, Λ_t, Λ_g, and Λ_d; a and b are constants. The central inset shows the direction of the flow and the orientation of the nearest neighbors in a regular cubic lattice.

specific emergent behaviors of this model are the expression of well-established physical processes. Finally, the numerical results are compared with observational data (section 5) to show that this CA model can be used to predict sediment fluxes on dune slopes as well as in dune fields.

2. Cellular Automaton Dune Model

[6] In a CA model for sediment transport, individual physical processes such as erosion, deposition and transport are implemented by nearest neighbor interactions and a time-dependent stochastic process. Simultaneously, a lattice gas CA model is used to compute the flow and quantify the bed shear stress on the topography. Then, the dependence of the erosion rate on the bed shear stress as well as the rebounds dynamics of fluid particles on sedimentary cells ensure permanent feedback mechanisms between flow and topography. A complete description of this model can be found in the work by *Narteau et al.* [2009]. We just recall here the main characteristics which are particularly relevant to the present study.

2.1. Cellular Automaton Model for Sediment Transport

[7] We consider a 3-D square lattice with three states (fluid, immobile sediment, sediment in motion) and nearest-neighbor interactions (Figure 2). An elementary cell is a cube of edge length l_0 and pairs of nearest neighbor cells are called a "doublet." For each individual physical process that we take into account, there is a set of doublet transitions. We have transitions for erosion (immobile sedimentary cells in contact with fluid cells are set in motion), deposition (sedimentary cells in motion become immobile), transport (motions of sedimentary cells with respect to fluid cells) and diffusion (lateral motions of sedimentary cells). Each transition is associated with a rate parameter with units of frequency ($1/t_0$) that introduces into the model the characteristic timescale of the corresponding physical mechanism [*Narteau et al.*, 2001]. Doublets are all supposed to be independent and the occurrence of a transition of doublet is assumed to follow a stochastic Poisson process. In practice, an iteration of the model corresponds to a single transition of doublet and a specific time step which are randomly chosen according to the local and the overall transition rate, respectively [see *Narteau et al.*, 2009, Appendix B]. Thus, by changing doublet by doublet the configuration of cells, we can study the morphodynamics of bedforms produced by the evolution of the population of sedimentary cells.

[8] To take into account gravitary effects (i.e., avalanches), we impose an angle of repose for the granular material. Actually, we do not allow two neighboring piles of sediment to have a height difference higher than l_0 (i.e., one cell). When it is the case, cells of the higher piles are redistributed and may produce avalanches according to the dynamics of the *Bak et al.* [1988] sand-pile model. Finally, in order to control all boundary conditions, we also use neutral cells to shape the geometry of our physical environment (e.g., solid bedrock, ceiling) as well as injection/removal cells to control the input/output fluxes of sediment, for example at the upstream/downstream borders.

2.2. Lattice Gas Cellular Automaton Model

[9] The flow is modeled via a lattice gas CA model. This type of discrete hydrodynamical models are based on motions of fluid particles than move from one lattice node to its neighbor in one unit of time [*Frisch et al.*, 1986; *d'Humières et al.*, 1986; *Chopard and Droz*, 1998]. Each particle has its own velocity vector (Figure 3a) and two particles cannot sit simultaneously on the same node if their direction are identical. One iteration is divided in two phases:

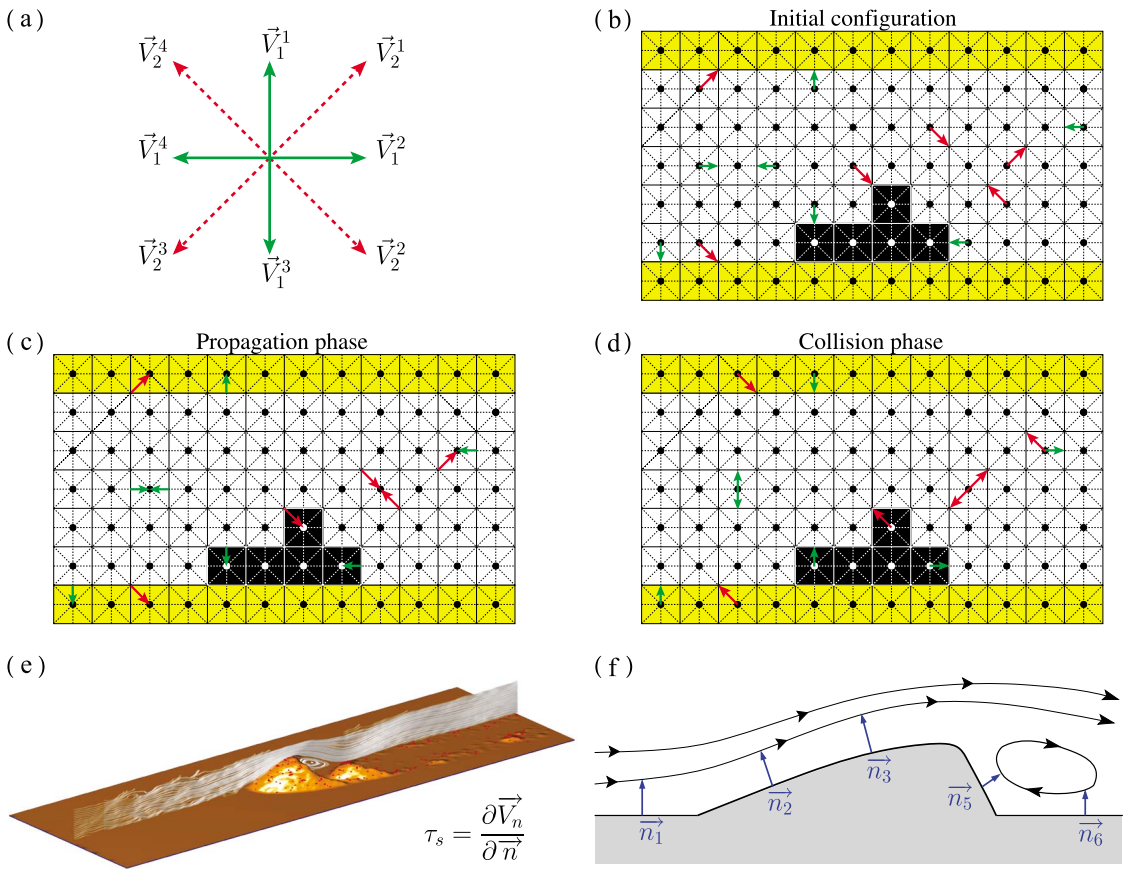

Figure 3. The lattice gas cellular automaton. (a) The possible velocity vectors for a fluid particle, $\|V_2^i\| = \sqrt{2}\|V_1^i\|$. Starting from (b) an initial configuration of fluid particles, an iteration of the model consists of (c) a propagation phase and (d) a collision phase. Particles and their velocity vectors are represented by arrows. Each cell of the model of sediment transport is represented by a dot in the center of a solid square (neutral cells are shown in yellow). Dashed lines are for connections between nearest and next-nearest neighbors. (e) Velocity streamlines above a barchan dune. Red dots are for sedimentary cells in motion. We observe the contraction of streamlines upstream of the crest of the dune and the divergence of streamlines that set up a recirculation zone above the slip face. (f) Schematic representation of the topography and the flow to show the normal to the topography along which we measure the bed shear stress.

during the propagation phase the particles move from their node to the nearest neighbor in the direction of their velocity vectors (from Figure 3b to Figure 3c); during the collision phase, particles on the same node exchange momentum if it is compatible with the imposed collision rules (from Figure 3c to Figure 3d). Then, during the computation, we can measure the velocity of the flow by averaging over space and time the different motions of fluid particles.

[10] For numerical efficiency, we only consider a set of equally spaced 2-D vertical lattices aligned with the direction of the flow. Between two planes, the vertical and horizontal components of the velocity field are obtained by linear interpolation.

2.3. Feedback Mechanisms

[11] The CA model for sediment transport and the lattice gas CA model can be used separately. Here, they are combined to simulate the complex interplay between a turbulent flow and a layer of erodible sediment lying on a solid flat bedrock (Figure 3e). These interactions are taken into account as follows.

[12] First, there is an effect of flow strength on the erosion rate Λ_e. In this purpose, we locally determine the bed shear stress:

$$\tau_s = \tau_0 \frac{\partial \vec{V}}{\partial \vec{n}}, \tag{1}$$

where τ_0 is the stress scale of the model, $\vec{V}$ is the velocity field expressed in terms of a number of fluid particles and $\vec{n}$ is the normal to topography (Figure 3f). Then, we consider that the local erosion rate is proportional to the viscous drag force exerted by the fluid on the particles. For a turbulent flow, it is therefore linearly related to the bed shear stress τ_s by

$$\Lambda_e = \begin{cases} 0 & \text{for } \tau_s \le \tau_1, \\ \Lambda_0 \dfrac{\tau_s - \tau_1}{\tau_2 - \tau_1} & \text{for } \tau_1 \le \tau_s \le \tau_2, \\ \Lambda_0 & \text{else,} \end{cases} \tag{2}$$

where τ_1 is a threshold of motion inception and τ_2 is a slope parameter. Note that, in practice, the erosion rate is not saturated because we always have $\tau_2 \gg \tau_s$. Thus, the characteristic time required to set in motion immobile sedimentary cells is inversely proportional to the excess shear stress value $(\tau_s - \tau_1)$.

[13] Second, there is an effect of topography on fluid flow through the rebound dynamics of the fluid particles. Indeed, these particles can only move within the fluid state of the CA of sediment transport. When they collide with the sedimentary or neutral cells that compose the bed, they rebound in the opposite direction in order to respect the conventional no-slip boundary conditions at a solid-fluid interface (Figures 3a–3d). Thus, any modification of the topography modifies the flow and subsequently the bed shear stress. On the other hand, because the flow is confined by a flat ceiling of neutral cells, the top boundary layer is set to free-slip conditions: rebounds are in the opposite direction for the vertical component of the velocity vector, but not for the horizontal component. Thus, fluid particles conserve their momentum in the direction of the flow (Figures 3a–3d). Finally, using equation (2) and the different aspects of the rebound dynamics, we end up with a fully coupled system where hydrodynamics and morphodynamics result from a combination of interactions between the elements of the system over time.

2.4. Scaling and Flow Strength

[14] As a preliminary work, *Narteau et al.* [2009] tested the stability of simple configuration of bedforms perturbed by sine wave to find the most unstable wavelength for the formation of dunes in the model. This wavelength expressed in units of cell length (i.e., l_0) can be compared with observations in order to determine the l_0 value. Thus, the elementary length scale of the CA dune model is dimensionalized with respect to the physical mechanism that select $\lambda_{\max}$, the characteristic length scales for the formation of dunes in nature. Then, in all natural environments where the dune instability can be observed, the l_0 value can be calculated with respect to the magnitude of the parameters that control the $\lambda_{\max}$ value [*Hersen et al.*, 2002; *Elbelrhiti et al.*, 2005; *Charru*, 2006; *Claudin and Andreotti*, 2006]. For example, if the model is used to reproduce aeolian dunes in arid regions on Earth, we have $l_0 \approx 0.5$ m for a mean grain diameter of 180 μm.

[15] For an ideally flat sand bed in a transport limited regime, a given flow velocity is associated with a constant bed shear stress and a quasi-stationary sediment flux, the so-called saturated flux Q_{sat}. We take advantage of these direct relationships to reproduce different flow conditions in the model. In practice, we only change the threshold shear stress value τ_1. Thus, we modify the excess shear stress, $\tau_s - \tau_1$, the main ingredient that controls transport through the erosion rate Λ_e (equation (2)). To relate the τ_1 value to a given flow velocity u_*, *Narteau et al.* [2009] derived from theoretical transport relationships that

$$\frac{Q_{\text{sat}}}{Q_{\text{sat}}^0} = 1 - \left(\frac{u_{\text{c}}}{u_*}\right)^2, \tag{3}$$

where Q_{sat}^0 is the Q_{sat} value for $\tau_1 = 0$ and u_{c} is a threshold velocity below which the flow cannot dislodge particles from the bed. Then, equation (3) and the Q_{sat} (τ_1) rating curve can be used to determine the flow velocity that corresponds to a specific τ_1 value, and vice versa [see *Narteau et al.* 2009]. Using these values, we can determine the characteristic timescale of the model from a direct comparison of the sediment fluxes in the model and in nature. Practically, assuming that we already know the l_0 value, the t_0 value is derived from the equation that relates the simulated flux expressed in units of l_0^2/t_0 to an observed flux expressed in m^2/s.

3. Morphodynamics of Barchan Dunes

[16] In 3-D simulations, we always consider a lattice of cells with a square base of side L_s and a height H_s (Figure 4a). Except for the τ_1 value that controls the strength of the flow, all the parameter values are kept constant (see Table 1) and equal to those used by *Narteau et al.* [2009].

3.1. Formation of Steady State Barchan Dunes

[17] First, we describe the formation of a steady state barchan dune in a tunnel. This tunnel has a flat bedrock, a ceiling and is laterally limited by two vertical walls of neutral cells facing each other at a distance of $L_s/2$. The downstream border is made of removal cells to eliminate all sedimentary cells that reach this limit. At the upstream border, a line of injection cell is inserted in the ceiling in order to reinject uniformly all the sedimentary cells that have been removed at the opposite border. The initial condition consists of a square pile of sediment with a side length of $L_s/4$ placed upstream in the center of tunnel (Figures 4b and 4c).

[18] Figure 4d shows the evolution of this sediment pile for $\tau_1 = 0$. Over a short time, avalanches produce a truncated pyramidal shape from which sedimentary cells are randomly dislodged. From these initial perturbations, elementary dune patterns grow and propagate on the pyramid's plateau. From a hydrodynamic point of view, stoss and lee slopes are characterized by contraction and dilation of the velocity streamlines, respectively (Figure 5a). As the superimposed dunes propagate and disappear, horns develop on both sides and the upstream face grows in height due to the accumulation of the sedimentary cells which are systematically reinjected into the system. Finally, a single surface area is exposed to the flow, a major slip face develop on the lee side and the entire structure rapidly reaches a steady state which is commonly describes as a crescentic barchan dune. As this evolution proceeds, secondary bedforms systematically develop along horns and smaller barchan dunes regularly form and detach.

[19] Figure 5b shows the velocity streamlines above the barchan dune. Not surprisingly, there is a convergence of streamlines on the face exposed to the flow. Downstream of the highest point, streamlines diverge and set up a recirculation zone above the slip face. According to equation (1), these streamline patterns explain why the bed shear stress is continuously increasing on the upstream face and why it is so low, and even negative, downstream of the dune crest (Figure 5c). Such variations are responsible for erosion and transport on the face exposed to the flow (i.e., Q_{sat} increases if $\partial\tau_s/\partial x > 0$) as well as for deposition on the slip face (i.e., Q_{sat} decreases if $\partial\tau_s/\partial x < 0$). Thus, the dune moves in the direction of the flow through the motion of grains from the

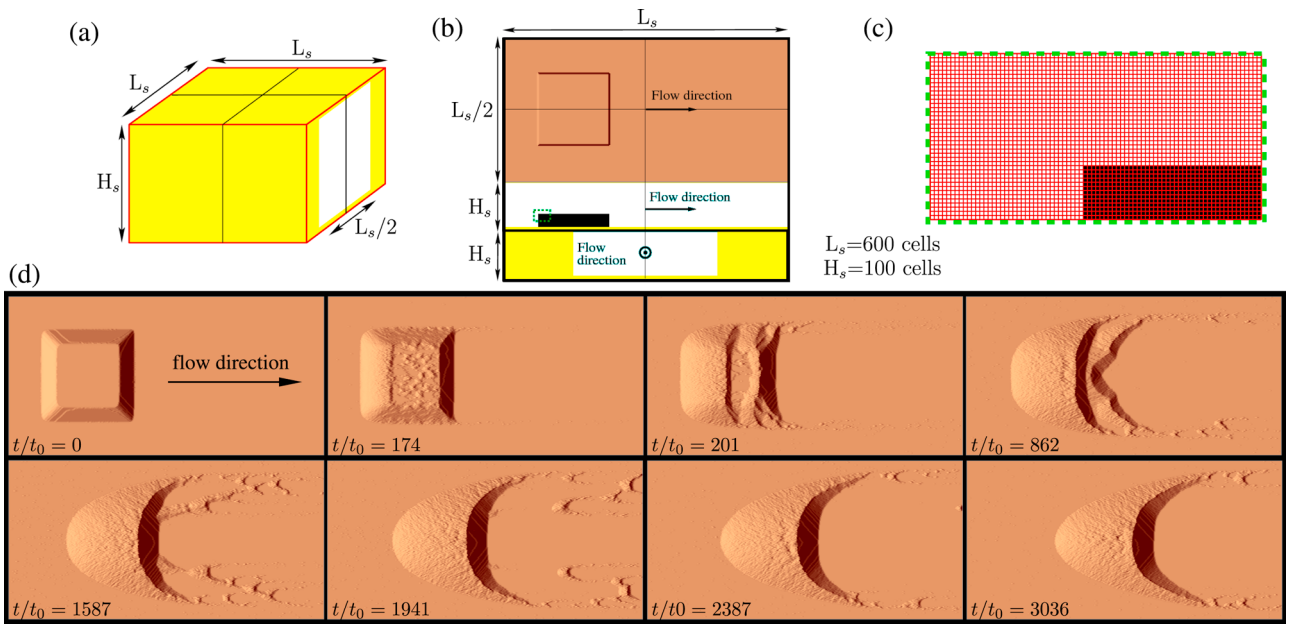

Figure 4. Evolution of a square pile of sediment in a tunnel of length L_s = 600 l_0 and width $L_s/2$ for τ_1/τ_0 = 0. (a) Geometry of the tunnel in the 3-D lattice of cells (neutral cells are shown in yellow). (b) The initial topography in the tunnel (top) and two vertical layers of cells parallel (middle) and perpendicular (bottom) to the direction of the flow (these two planes are shown with black lines in Figure 4a). (c) A zoom on the pile of sediment (see the dashed box in Figure 4b) to distinguish active doublets at t/t_0 = 0. (d) Evolution of an initial square pile of sediment until the crescentic barchan shape reaches a steady state (see text).

bottom to the top of the upstream face and their accumulation on the lee side. As in nature, Figure 5d shows also a reduction in shear stress at the toe and upstream of the dune [*Howard et al.*, 1978; *Wiggs et al.*, 1996; *Sauermann et al.*, 2001].

[20] Figure 5c shows that oscillations of the bed shear stress at the top of the dune correspond to a similar but smaller waveform pattern in the topography (see Figure 4d at t/t_0 = 3036). These secondary dune features have a wavelength of approximately 40 l_0 similar to the initial length of the instability observed along the horns where smaller barchan dunes form and detach (Figure 5e). According to *Narteau et al.* [2009], these observations suggest that different generations of dunes are governed by the same physical processes. Furthermore, it also indicates that the internal dynamic of dunes may lead to a hierarchy of structures [*Andreotti et al.*, 2009].

[21] To examine dune calving and the origin of secondary bedforms, we plot space-time diagrams of the dune height along vertical cross sections parallel to the direction of the flow and cutting through the horns (Figure 6). In these diagrams, a diagonal stripe pattern confirms that the detachment mechanism is associated to superimposed bedforms that propagate along dunes. As pattern coarsening occurs during this propagation, this is only when these secondary bedforms have an amplitude comparable to dune height that smaller dune features can detach. For the same reason, superimposed dune patterns are more likely to be observed at the dune termination, where horns are lower and narrower (compare Figures 6a and 6c).

[22] Figure 1 shows that similar dune patterns may be observed in nature. Nevertheless, changes in direction of the flow, variations in sediment supply and interactions with other dunes produce more complicated structures. It is not in the scope of the present paper to reproduce in details all these patterns. Instead, we investigate different flow strengths under which they are more likely to form.

Table 1. Units and Values of the Parameters of the Model of Sediment Transport[a]

Elementary Units	Units	
l_0, length	$[L]$	
t_0, time	$[T]$	
τ_0, stress	$[M][L]^{-1}\,[T]^{-2}$	
Model Parameters	**Units**	**Value**
L_s, system width and length	l_0	[400,600]
H_s, system height	l_0	100
Λ_0, transition rate for erosion	$1/t_0$	1
Λ_t, transition rate for transport	$1/t_0$	1.5
Λ_c, transition rate for deposition	$1/t_0$	0.5
Λ_g, transition rate for gravity	$1/t_0$	10^5
Λ_d, transition rate for diffusion	$1/t_0$	0.01
a, erosion/transport coefficient	1	0.1
b, deposition coefficient	1	10
$\tau_2 - \tau_1$, erosion range	τ_0	100

[a]Transition rates for erosion, deposition, and transport are chosen close to 1 with $\Lambda_c < \Lambda_0 < \Lambda_t$. Gravity (Stokes' law) and diffusion are occurring over much shorter and longer periods of time, respectively. We chose $\Lambda_c \ll \Lambda_0 \ll \Lambda_t$. The value $a < 1$ corresponds to the ratio between vertical and horizontal transition rates for erosion and transport; $b > 1$ corresponds to the ratio between deposition rates on flat and rough surfaces (see Figure 2).

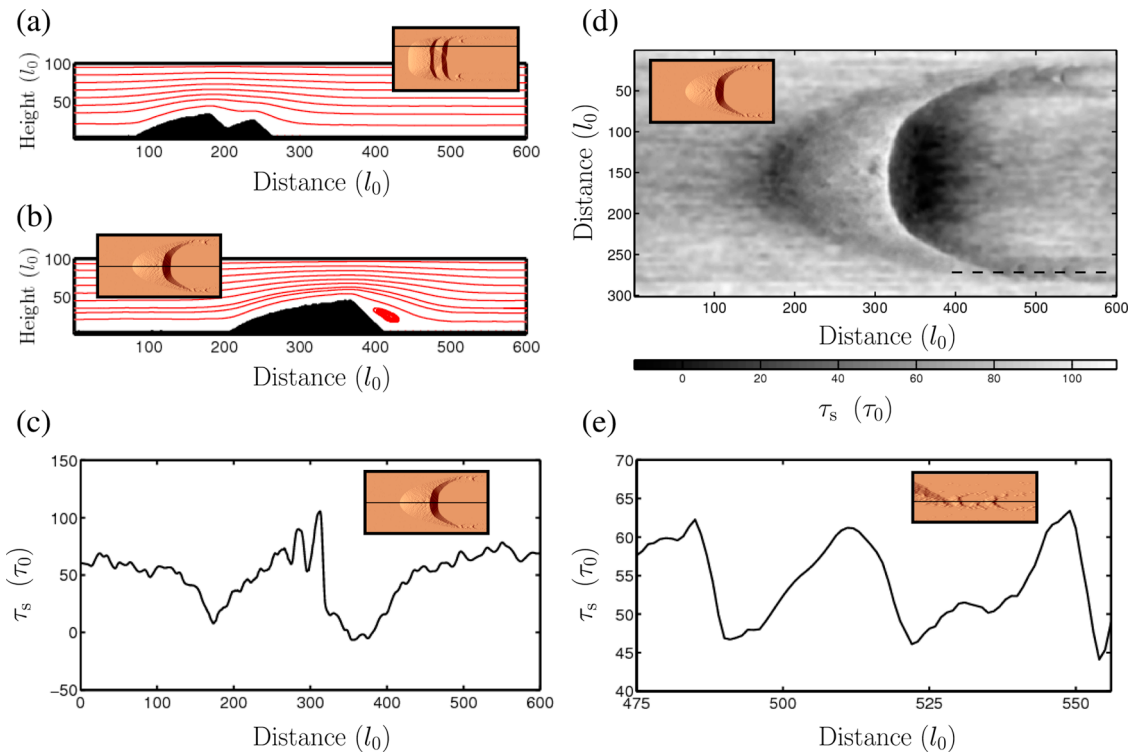

Figure 5. Velocity streamlines and bed shear stress during the formation of the barchan dune shown in Figure 4. (a) Velocity streamlines in a vertical plane parallel to the direction of the flow at $t/t_0 = 460$. (b) Velocity streamlines in a vertical plane parallel to the direction of the flow at $t/t_0 = 4250$. (c) The bed shear stress along a vertical cross section parallel to the direction of the flow ($t/t_0 = 3036$). (d) The bed shear stress across the entire domain ($t/t_0 = 3036$). (e) The bed shear stress along a vertical cross section passing through a horn (see dashed line in Figure 5d). For each plot, an inset shows the corresponding dune topography and, if necessary, the section along which the physical quantities have been evaluated.

[23] In what follows, we see the effect of lower flow conditions taking $\tau_1/\tau_0 = 20$ and the same initial conditions than in Figure 4. In comparison, Figure 7a shows the steady shape of the barchan dune: its height is shorter and its main body is more elongated. The main reason for these changes in morphology is that the base of the dune is less frequently above the erosion threshold. Then, there is a higher increase in sediment flux between the dune toe and the crest with a

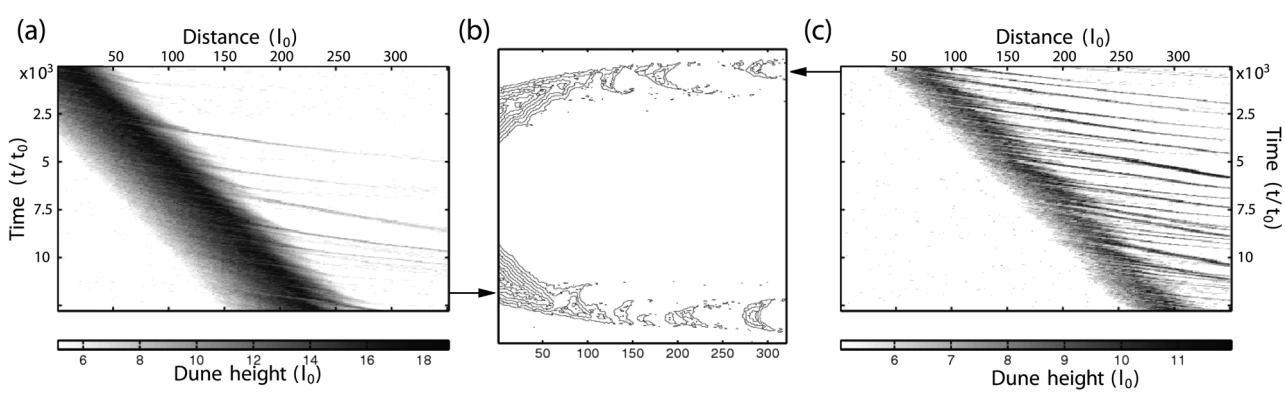

Figure 6. Space-time diagrams of dune height along horns. (a) The topography measured along a vertical cross section parallel to the direction of the flow at 100 cells from the center of the dune. The arrow between Figures 6a and 6b shows the location of this plane. (b) A zoom on the dune patterns along the horns: smaller dunes form and detach as a result of the propagation of superimposed bedforms along the horns. (c) The topography is measured along a vertical cross section parallel to the direction of the flow at 120 cells from the center of the dune. The arrow between Figures 6b and 6c shows the location of this plane.

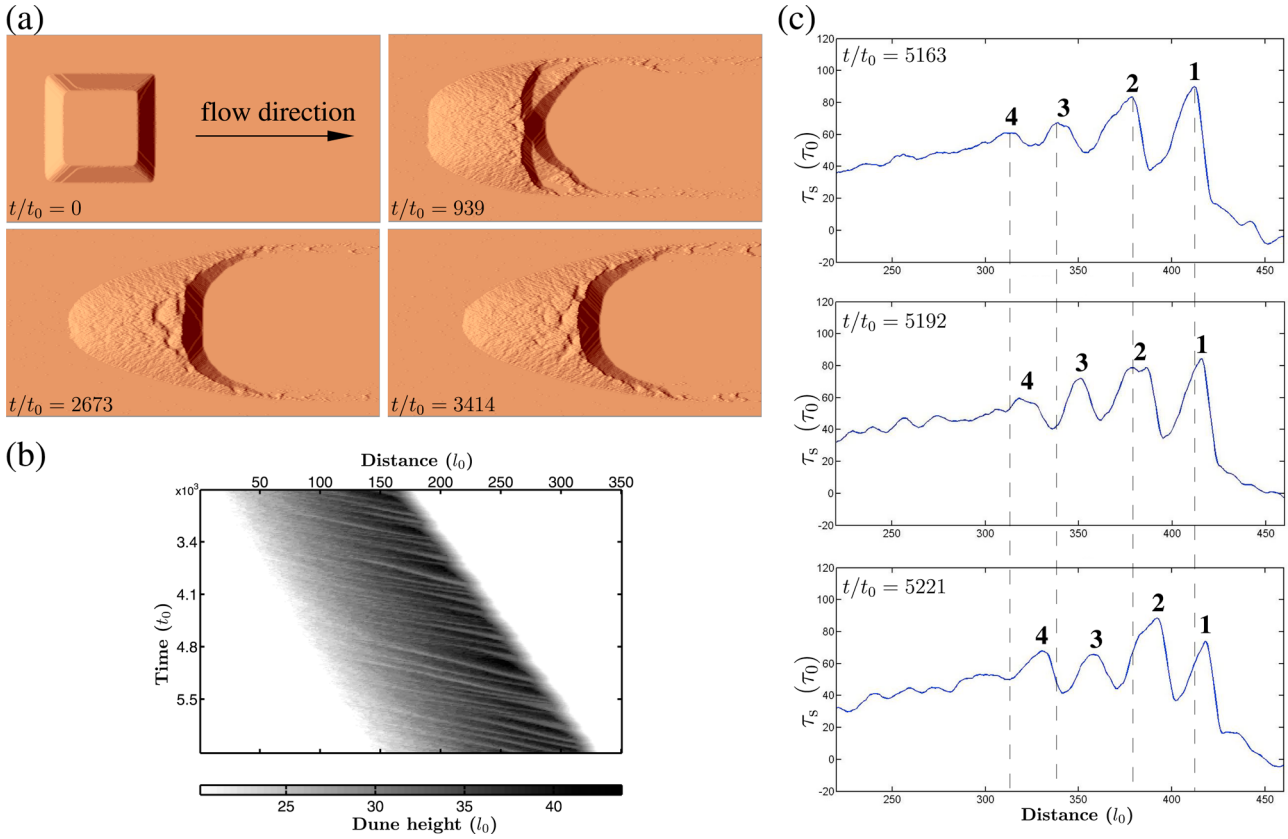

Figure 7. (a) Evolution of an initial square pile of sediment until the crescentic barchan dune reaches a steady state for $\tau_1/\tau_0 = 20$. From the comparison with Figure 4, we observe that, in the model, dune shape depends on flow strength. (b) Space-time diagram of the topography measured along a vertical cross section parallel to the flow and cutting through the center of the dune. Each stripe can be associated to a superimposed dune. The propagation speed of this dune is given by the slope of the stripe. (c) The bed shear stress along a vertical cross section parallel to the direction of the flow cutting through the center of the dune. With the numbers and the dashed lines we can follow four peaks at three different times and observe the propagation of superimposed bedforms.

decreasing flow strength. As a consequence, the dune is stretched in the direction of the flow.

[24] Dynamically, the major difference at low flow is the increase in amplitude of the superimposed bedforms. In fact, these secondary dune patterns are enhanced by a more gradual slope along the upstream face. Figure 7b shows that these new dunes form at a constant rate from the dune toe. Then, they propagate, grow and merge with each other until they collapse in the form of avalanches when they reach the main slip face. Along cross sections parallel to the flow, we determine the position of the wave peaks of the bed shear stress at the top of the dunes (Figure 7c). The distance between two peaks is almost constant and, one more time, a characteristic wavelength of about 40 l_0 can be observed.

3.2. Morphodynamics of Isolated Barchan Dunes With Superimposed Bedforms

[25] To investigate the influence of flow strength and dune size on the morphodynamics of barchan dunes, we run a series of 2-D numerical simulations. Thus, there is no lateral flux of sediment, either through avalanches or diffusion [*Hersen*, 2004]. More importantly, we can directly compare our predictions with quasi 2-D subaqueous barchan dunes observed in laboratory experiments [*Groh et al.*, 2008, 2009]. As in the model, these experiments have been conducted under confined and unidirectional flow conditions. Three Reynolds number regimes have been considered, $Re = \{25500, 27000, 28500\}$, using distilled water and glass beads with a density of 2.5 g/cm^3 and a mean diameter of 580 μm.

[26] In our simulations, we use three threshold shear stress values, $\tau_1/\tau_0 = \{0, 10, 20\}$, to reproduce high, intermediate and low flow strengths. For each of them, we consider the same set of initial conditions to explore a range of dune size similar to that observed in the laboratory experiment. In practice, we take l_0 = 1.7 mm. For this estimation, we use the characteristic length scale $\lambda_{\max} \approx 40\ l_0$ for the formation of dunes in the model [*Narteau et al.*, 2009] and the scaling proposed by *Claudin and Andreotti* [2006]:

$$\lambda_{\max} \approx 50\,\frac{\rho_s}{\rho_f}\,d, \tag{4}$$

where ρ_s/ρ_f is the sediment to fluid density ratio and d is the grain diameter [see also *Hersen et al.* 2002].

[27] As the simulation proceeds, the barchan shape emerges and the dune reaches a steady state characterized by its

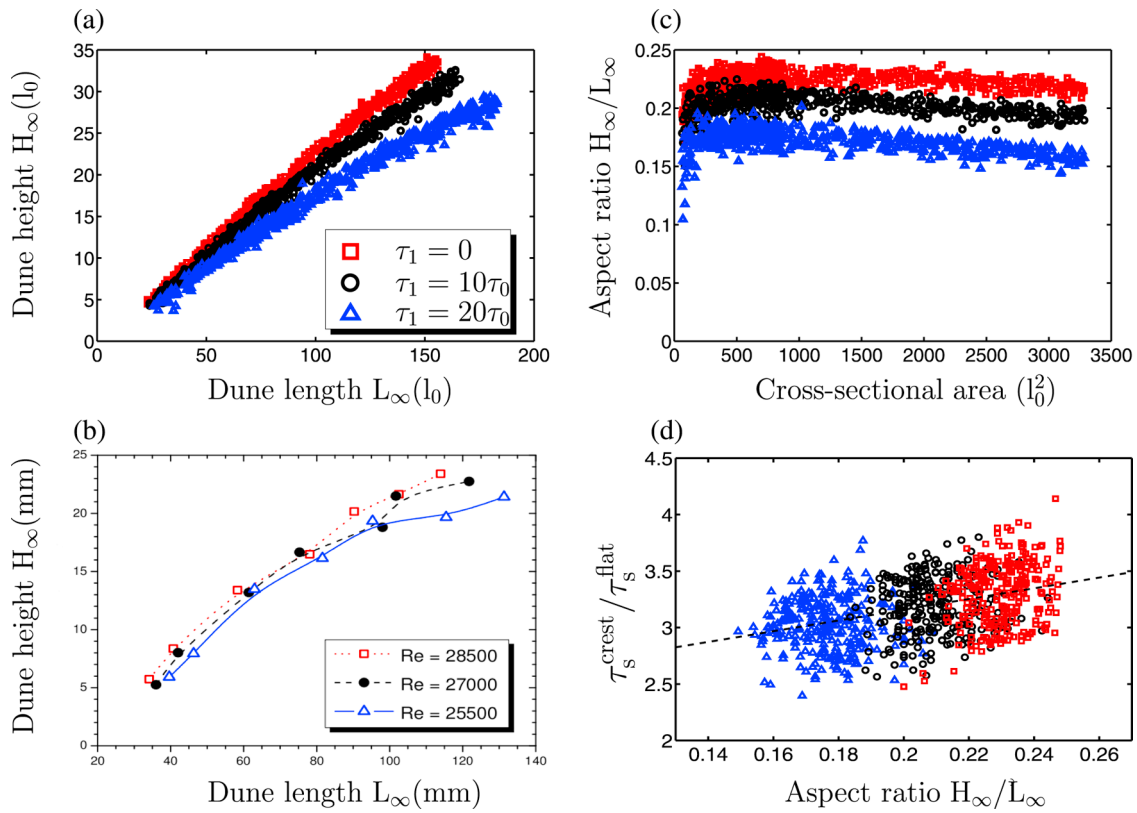

Figure 8. Morphodynamics of 2-D barchan dunes in a steady state. (a) Dune height as a function of dune length. (b) Dune height as a function of dune length in laboratory experiments for three Reynolds numbers: Re = 25,500; Re = 27,000; and Re = 28,500 [*Groh et al.*, 2008]. (c) Dune aspect ratio as a function of the volume of the dunes. (d) Increase in bed shear stress at the top of the dunes as a function of their aspect ratio. The dashed line is the best regression line (equation (5)). As we average the bed shear stress over a long time for a given topography, the dispersion of points is mainly due to the presence of superimposed bedforms. Except for Figure 8b, red squares, black circles, and blue triangles are for τ_1/τ_0 values equal to 0, 10, and 20, respectively.

length L_∞, height H_∞, volume V_∞, and velocity c. Figure 8a shows the evolution of dune height with respect to dune length for the three different flow strengths. As in laboratory experiments (Figure 8b), dune height increases with flow strength and there is not a linear relationship between dune length and dune height. Then, the aspect ratio H_∞/L_∞ is not a constant. It increases with the strength of the flow and, except for the smallest dunes, it decreases with the volume of the dune (Figures 8c). These changes in morphology affect the velocity field and, for all steady state barchan dunes, we measure the bed shear stress at the crest of the dune, τ_s^{crest} and upstream of the dune on a flat surface, τ_s^{flat}. Figure 8d shows that the increase in bed shear stress between the ground and the crest is directly proportional to the aspect ratio of the dune,

$$\frac{\tau_s^{crest}}{\tau_s^{flat}} = 5.07\frac{H_\infty}{L_\infty} + 2.30. \tag{5}$$

Despite some fluctuations due to the presence of superimposed bedforms, this observation is in good agreement with theoretical predictions [*Jackson and Hunt*, 1975] and field observations [*Lancaster*, 1985].

[28] Under unidirectional flows, it can be shown from the equation of mass conservation that stable dunes migrate in the downwind direction with a velocity that depends on their size [*Bagnold*, 1941]. For a dune with a well-established recirculation zone that captures all the sediment that pass through the crest, it is generally admitted that its migration speed c is inversely proportional to its height [*Elbelrhiti et al.*, 2005], length [*Kroy et al.*, 2002] or width [*Elbelrhiti et al.*, 2008]. Unfortunately, the field data are not accurate enough to distinguish between these different length scales. Arbitrarily, we use here the height H and an inverse scaling of the form

$$c = \frac{Q_{sat}^{crest}}{H + H_0}, \tag{6}$$

where Q_{sat}^{crest} is the saturated flux measured at the dune crest and H_0 is a height constant that removes the singularity at $H = 0$. Physically, the H_0 value can also be considered as the parameter that sets the velocity of the smallest dunes [*Elbelrhiti et al.*, 2005]. Equation (6) can be rewritten

$$c = \frac{aQ_{sat}^{flat}}{H + H_0}, \tag{7}$$

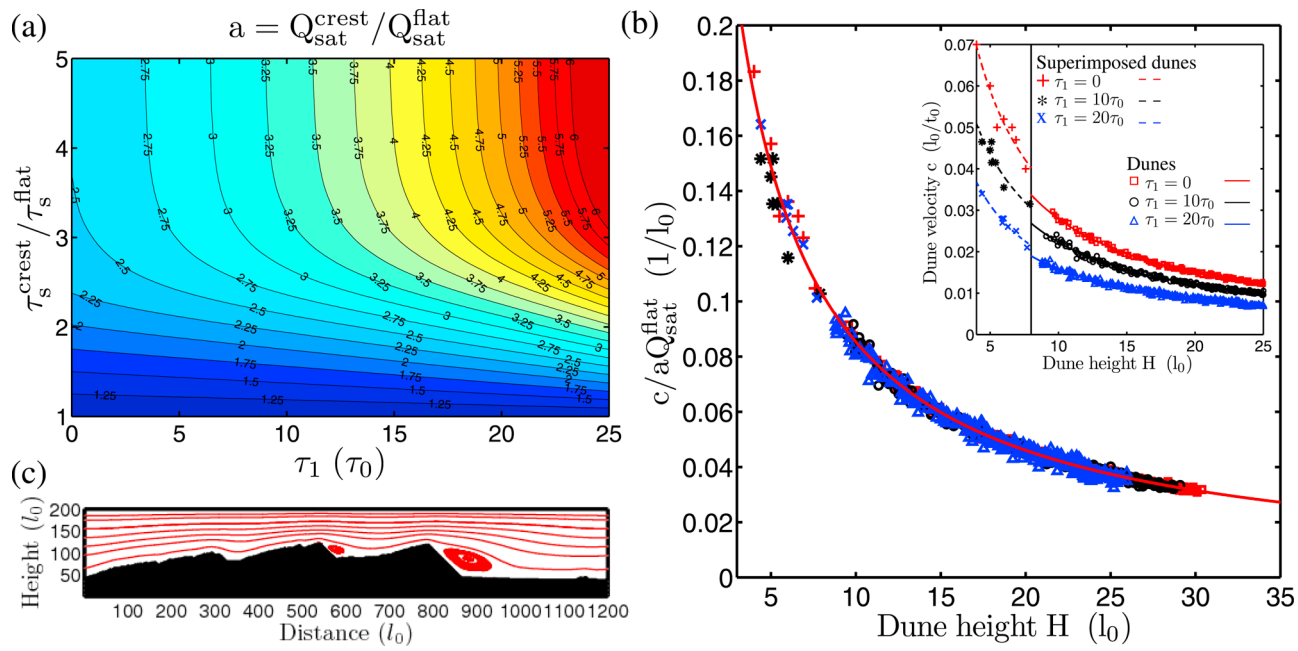

Figure 9. (a) The increase in sediment flux between the ground and the crest as a function of two parameters: the flow strength (i.e., negatively correlated with τ_1) and $\tau_s^{crest}/\tau_s^{flat}$, the increase in bed shear stress between the ground and the crest. (b) The propagation speed of dunes ($H > 8$) and superimposed bedforms ($H \leq 8$) rescaled with respect to the sediment flux at the crest for three different flow strengths (red, black, and blue symbols are for τ_1/τ_0 values equal to 0, 10, and 20, respectively). The line is the best fit of $1/(H + H_0)$ to the data with $H_0 = 1.71\ l_0$. The inset shows the raw data without rescaling. Lines are the best fit of equation (6) to the data. For dunes and for an increasing flow strength, we have $Q_{sat}^{crest} = 0.19$, $Q_{sat}^{crest} = 0.26$, and $Q_{sat}^{crest} = 0.33$ in units of l_0^2/t_0 and $H_0 = 1.9$, $H_0 = 1.7$, and $H_0 = 1.8$ in units of l_0. For superimposed bedforms, we have $Q_{sat}^{crest} = 0.21$, $Q_{sat}^{crest} = 0.30$, and $Q_{sat}^{crest} = 0.38$ in units of l_0^2/t_0 and $H_0 = 1.6$, $H_0 = 2.0$, and $H_0 = 1.5$ in units of l_0. (c) Velocity streamlines above a giant dune with two generations of superimposed bedforms. Note the formation of a secondary recirculation zone.

where Q_{sat}^{flat} is the saturated flux measured upwind of the dune and a is the increase in flux between the ground and dune crest. Nevertheless, in this case, the a value is supposed to be a constant directly related to the scale-invariant shape of dunes. In our model, the situation is different because we have shown that the dune aspect ratio varies with respect to flow velocity and dune size (Figure 8). Then, we directly compute the a value with respect to the τ_1 value (i.e., the flow strength) and with respect to the increase in bed shear stress between the ground and the dune crest (Figure 9a). Interestingly, we find that the a value increases with decreasing flow strength and steeper stoss slopes.

[29] The inset of Figure 9b shows the velocity of steady state dunes as a function of their heights for $H > 8\ l_0$ and three different flow strengths. For $H < 8\ l_0$, we also plot the propagation speed of superimposed bedforms on the top of these dunes. Not surprisingly, dunes are faster at higher flow velocities, and equation (6) fits well with the numerical data. The Q_{sat}^{crest} value increases with an increasing flow velocity (see values in the caption of Figure 9). For dunes and superimposed bedforms (Figure 9c), H_0 values do not depend of flow velocity and have a mean value of $1.7 \pm 0.2\ l_0$. Because the bed shear stress increases on the upstream face of the dune, superimposed bedforms are faster than dunes with the same height propagating on a flat bedrock. As shown in Figure 9b, the dune velocity can be rescaled by aQ_{sat}^{flat}, the increase in flux between the ground and the crest (equation (7)). In this case, dunes and superimposed bedforms follow the same law with the same parameter $H_0 \approx 1.7\ l_0$, suggesting again that these dune features are different expressions of the same physical mechanisms.

[30] These 2-D computations show that, if they were independent, different slices of 3-D barchan dunes would not propagate at the same speed. Hence, in order to reach a steady state, lateral flux of sediment directed from higher (slower) to lower (faster) parts of the barchan are required. In the model, these lateral motions of sedimentary cells are provided by avalanches and diffusion (see Figure 2). In practice, the diffusion rate constant Λ_d determines the stable slope profiles of dunes as in models that use a set of partial differential equations [*Hersen*, 2004]. Theoretically, it is because the time evolution of the probability density function associated with the position of the particle undergoing a Brownian movement can be well approximated by a diffusion equation. In section 4, we use transverse dunes to illustrate in more details the impact of avalanches and diffusion on the dynamics of dune fields.

3.3. Morphodynamics of a Population of Barchan Dunes

[31] In order to study the formation and the evolution of a population of barchan dunes, $9 \cdot 10^5$ sedimentary cells are

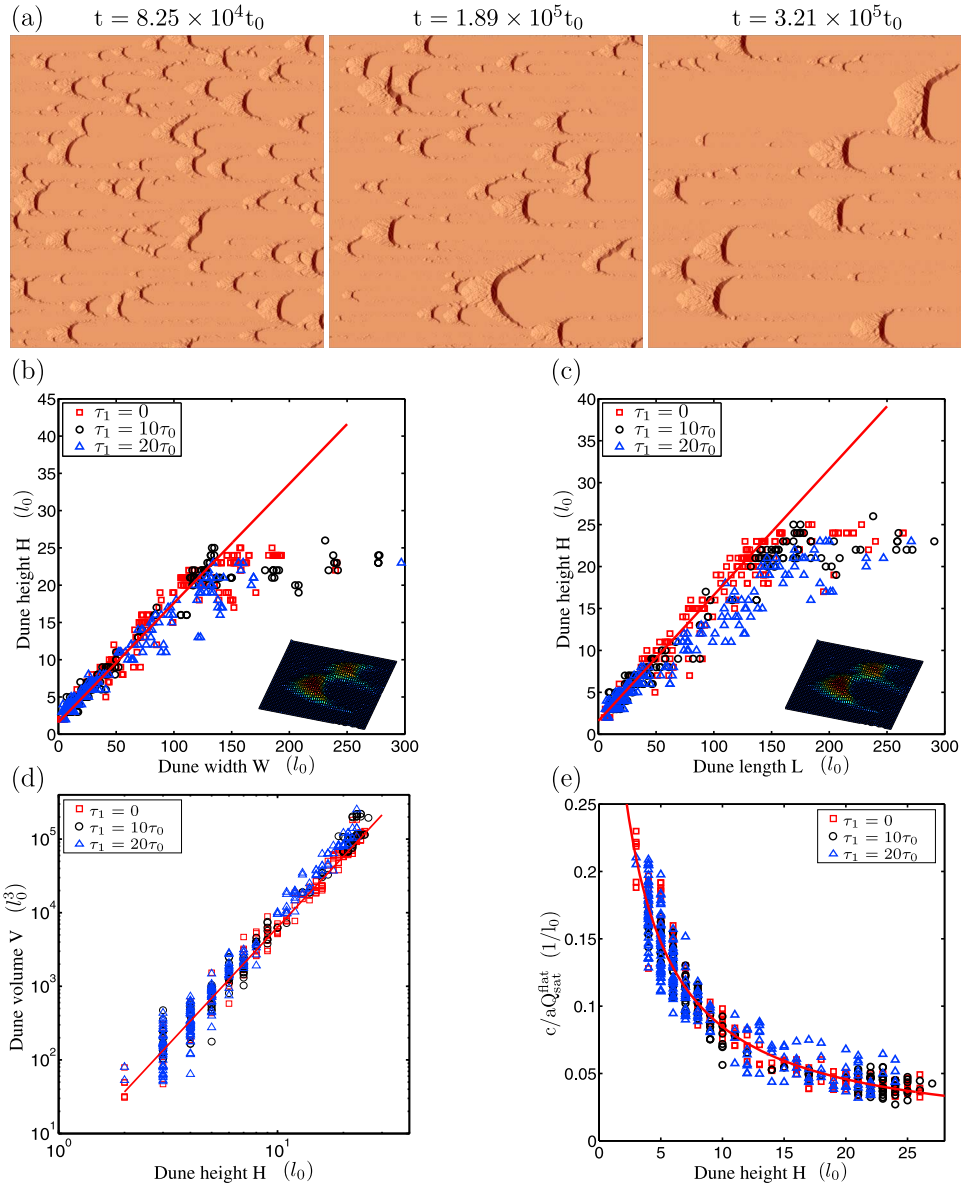

Figure 10. Statistical relationships in barchan dune fields for different flow strengths. (a) Formation and evolution of a barchan dune field for $\tau_1/\tau_0 = 20$. (b) Dune height as a function of their width: the solid line is the best linear fit, $H = 0.14W + 1.5$. (c) Dune height as a function of their length: the solid line is the best linear fit, $H = 0.16L + 1.6$. As shown in the insets of Figures 10b and 10c, lateral linking explains largest width values. (d) Dune volume as a function of their height: the solid line is the best power law fit $V \approx 6.2H^3$. (e) Propagation speed rescaled by the flux at the crest as a function of dune height: the solid curve is the best fit with $c/(aQ_{\mathrm{sat}}^{\mathrm{flat}}) = 1/(H + 1.9)$. Red squares, black circles, and blue triangles are for τ_1/τ_0 values equal to 0, 10, and 20, respectively.

randomly distributed on a square ground plane of side length $L_s = 10^3\ l_0$. We use periodic boundary conditions and we stop computations when large dunes start to interact with themselves across the entire domain. Under the stationary conditions of the system (flat bedrock topography, constant flow strength and direction), collisions mainly result in the formation of larger structures by amalgamation. As a result, the average size of barchan dunes is always increasing (Figure 10a), and Figure 10a shows three different stages of dune growth. At each stage, as in Figure 1e, we recognize complex dune-dune interaction with collisions, merging, lateral linking as well as repulsion [*Kocurek and Ewing*, 2005]. Superimposed bedforms are ubiquitous and, as for isolated barchans, the formation and the detachment of smaller barchans along horns are frequent. Such behavior is amplified by collisions and can produce swarms of smaller barchan dunes downstream (Figure 1a). In addition, we can identify zones where the dunes are affected by perturbation of the flow induced upstream by other topographic features. This suggests that dune populations are not only controlled by mass exchanges during collision, but also by long-range interactions related to turbulent flow properties.

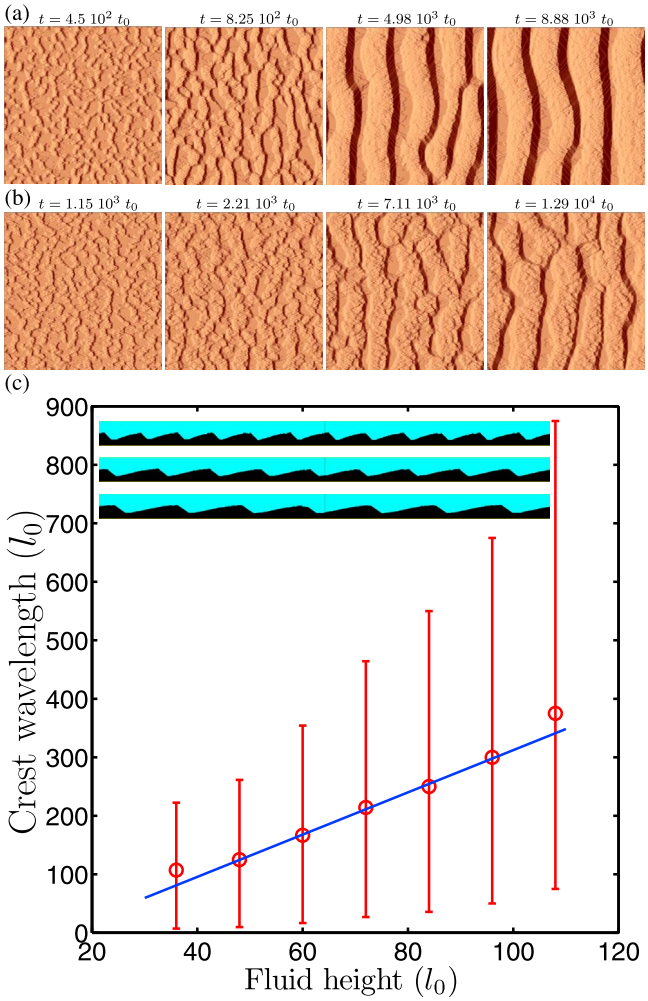

Figure 11. Formation and evolution of transverse dune fields for (a) $\tau_1/\tau_0 = 0$ and (b) $\tau_1/\tau_0 = 20$. (c) The crest-to-crest wavelength of stable transverse dune fields as a function of flow depth in 2-D simulations. In practice, this wavelength is given by L/n_c, where L and n_c are the length of the system and the number of crests in the direction of the flow (here $L = 1.5 \times 10^3\ l_0$). Error bars correspond to $n_c \pm 1$ crests.

[32] At different times and for the different flow strengths, we measure the height H, length L and width W of all the barchan dunes within the dune field. Figure 10 shows that linear relationships fit reasonably well the relations between H, L and W. It follows that the dune aspect ratio H/L can have a constant value with an increasing flow strength and for dunes of different sizes (Figure 10a). Given the level of noise that result from complex dune-dune interactions, this result is not in contradiction with the result shown in Figure 8a. It rather indicates that barchans are not in a steady state because the dynamic equilibrium between flow and topography is permanently evolving in complex dune fields. The most stable parameter is the volume of barchan dunes which always scales as the cube of H, L or W, the linear dimensions of the dunes (Figure 10c). In addition, despite the fluctuations induced by collisions, the propagation speed of barchans rescaled by the sediment flux at the crest is inversely proportional to dune height (Figure 10d). Finally, the best fit of $1/(H + H_0)$ to the data gives a H_0 value of approximately 1.9 l_0 for all flow strengths.

4. Morphodynamics of Transverse Dune Fields

[33] Under uniform and unidirectional flow conditions without surface limiting factors (e.g., vegetation), there is a continuous transition of barchan into transverse dunes fields for an increasing sediment availability [*Livingstone and Warren*, 1996]. This is also the case in the model, and Figure 11 shows the formation and the evolution of transverse dune fields for $L_s = 400\ l_0$, $H_s = 100\ l_0$, periodic boundary conditions and two different flow strengths ($\tau_1/\tau_0 = 0$ in Figure 11a, $\tau_1/\tau_0 = 20$ in Figure 11b). As for barchan dunes, we observe superimposed bedforms and pattern coarsening. However, over a long time, transverse dune fields reach a steady state that can be characterized by a mean amplitude, a crest-to-crest wavelength and a crestline sinuosity.

[34] Here, it is important to note that the stabilizing process responsible for the limitation of dune size is not sediment availability. During the numerical simulations, transverse dunes always propagate on a deep layer of sedimentary cells and the solid bedrock is never exposed to the flow. Then, the key element for the limitation of dune size is the top boundary layer [*Andreotti et al.*, 2009]. In fact, using a flat ceiling with a free-slip boundary condition, transverse dunes cannot grow indefinitely because of the confinement of the flow. Then, for an infinite sediment availability, the characteristic wavelength and the amplitude of steady state transverse dune fields can be directly related to the average depth of the flow (Figure 11c).

[35] In the model, we observe that the sinuosity of crest lines strongly depend on the value of the lateral diffusion coefficient. For smaller value, when transverse fluxes are reduced, the bedforms three dimensionality increases because of defect migration and termination creation. Inversely, an increase of lateral fluxes limit height difference between two adjacent layers of cells and tend to form 2-D transverse dune fields (i.e., regular crestlines perpendicular to the flow).

[36] Figure 12 shows typical transverse dune patterns with respect to the Λ_d and τ_1 values to investigate the effect of diffusion and flow strength, respectively. In all cases, transverse dune fields are in a quasi-stationary steady state and, as in Figure 11, the solid bedrock composed of neutral cells is never exposed to the flow. Overall, Figure 12 shows that bedform three-dimensionality is increasing with a decreasing diffusion rate and a decreasing flow strength. If the role of diffusion is straightforward from what has been said in the previous paragraph about lateral sediment motion, the influence of flow strength on bedforms is less direct because it involves the retroaction between flow velocity and dune morphology as well as the lateral spreading of avalanches. Two behaviors in particular have to be highlighted: (1) dune height is greater under higher flow conditions, and (2) the size of avalanches tends to increase with the size of the dune, and there is therefore a positive correlation between dune height and lateral flux of sediment on the lee face slope. Combining these two behaviors, lateral flux of sediment increases with an increasing flow strength (i.e., lower τ_1

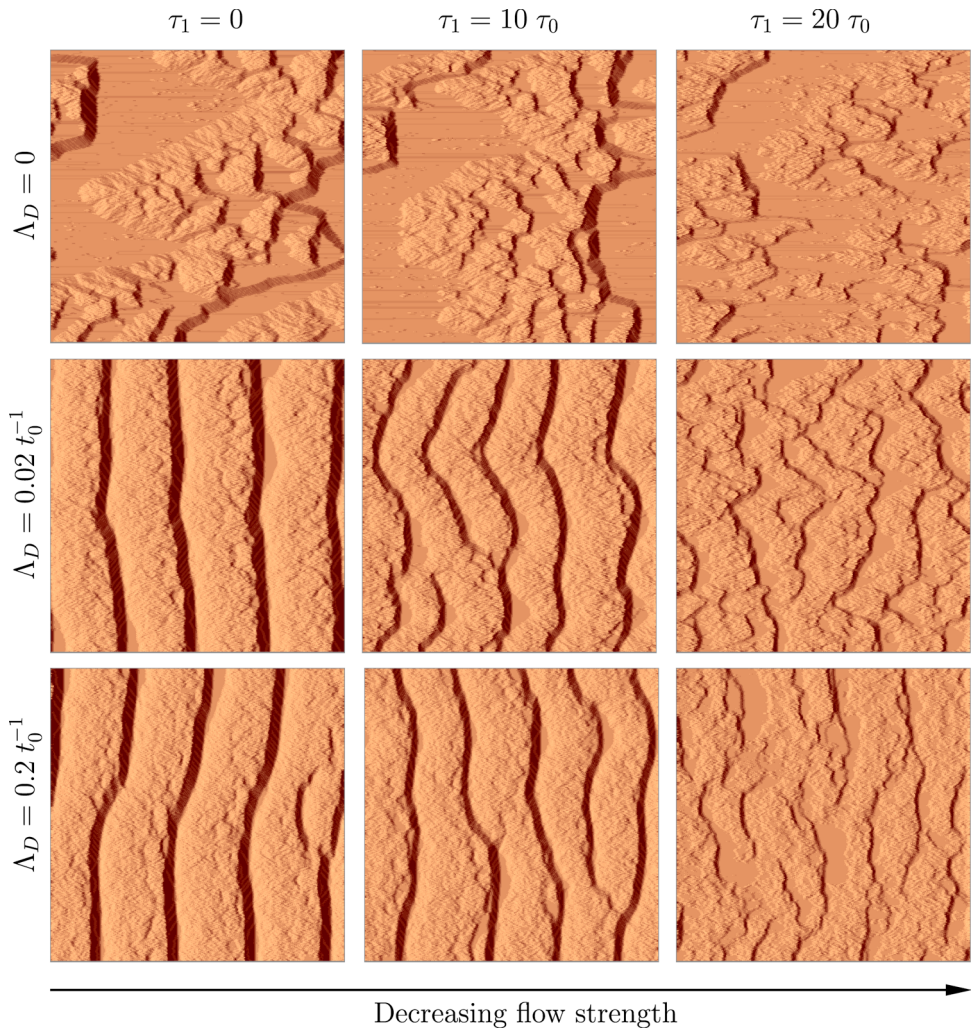

Figure 12. Stable transverse dune fields as a function of Λ_d and τ_1. Thus, we investigate the influence of diffusion (Λ_d) and flow strength (τ_1). Note the transition between 3-D and 2-D transverse dune fields as the lateral flux of sediment is increasing (see text for explanation).

value). Then, as for a decreasing diffusion rate, there is also a clear transition from 3-D to 2-D transverse dune fields when the flow velocity increases.

5. Concluding Remarks

[37] The present study focus on the morphodynamics of superimposed bedforms produced under unidirectional and confined flow conditions by a CA dune model. This model can be described as a real-space CA because the only information stored on each individual cell is a physical state which locally represents the different phases involved in the mechanics of sediment transport. In contrast with numerical methods that solve partial differential equations using a whole set of physical variables, the real-space representation technique offers the opportunity to implement codes which are entirely based on a combination of interactions between the elements of the system over time. Moreover, as for the continuous methods, we are also able to describe the entire system in terms of well-defined physical quantities (e.g., bed shear stress, sediment flux). Using them, we show that emergent behaviors of our system satisfy relations based on the current understanding of the mechanics of sediment transport. Then, in order to compare the output of the model with specific dune features in natural environments, we try to isolate the effect of different factors on the statistical steady state of dune fields. Namely, we first concentrate on sediment availability, flow strength, flow depth and lateral sediment motions.

[38] In the model, the amount of lateral sediment motion determines the stable shape of barchan dunes and transverse dune fields. In nature, these lateral motions involve a large variety of physical processes including grain-grain collisions and 3-D turbulent fluid flows [*Hersen*, 2004; *Sauermann*, 2001; *Schwämmle and Herrmann*, 2005]. In our numerical simulations, the diffusion rate combines all these processes together in a single parameter Λ_d. As a consequence, this parameter may be related to the flow strength as well as to any other parameter that participates to transport. For the sake of simplicity, we do not introduce such relations here; we prefer

consider Λ_d as a constant. Nevertheless, different types of dependences of diffusion rate on flow velocity can be envisioned from the dune field features exposed in Figure 12. Interestingly, such dependences may lead to either an increase or a decrease of the three dimensionality of bedforms. However, the quantitative analyses of defect propagation in transverse dune fields require an independent study in which the role of the top boundary layer in relation with the sediment availability needs to be addressed.

[39] In our numerical simulations, the stability of transverse dune fields results from a limitation in dune size. Without such a limitation, pattern coarsening, termination creation and defect propagation lead to different dune features according to sediment availability.

[40] 1. For an infinite amount of sediment, the only stable feature is a unique transverse dune with a height proportional to the size of the system.

[41] 2. If there is a limited amount of sediment, the bedrock will be exposed to the flow and the transverse dune fields will ultimately transform into a finite number of giant barchan dunes.

[42] This is for example the case for all transverse dune fields produced by the Werner's CA dune model or any other model that does not encompass a direct control of the flow on transport properties. Analyzing the steady state transverse dune fields produced by our model, we show that the crest-to-crest wavelength scales linearly with flow depth. Given the free-slip boundary conditions at the top of the system, this limitation in dune size results from the acceleration of the flow induced by the confinement as well as from changes in the distribution of the bed shear in the neighborhood of the crests during dune growth. Nevertheless, the underlying physical mechanism responsible for this stabilizing process is not in the scope of this paper because it is likely that a full answer will require a dedicated study. In fact, an important element of the challenge is that hydrodynamical properties and the stability of the fluid-bed interface needs to be explored using a free boundary layer at the top of the system [*Kennedy*, 1963; *Andreotti et al.*, 2009].

[43] A fortiori, the role of flow depth is also critical for the stability of barchan dunes. However, the results presented here for barchan dunes have been obtained with a flow depth much higher than dune height in order to eliminate the effect of confinement. Then, we observe that steady state barchan dunes are not scale invariant: their shape depend on flow strength and dune size. These changes in dune shape affect the dynamical behavior of dunes if, as predicted by *Jackson and Hunt* [1975], the change in bed shear stress between the ground and the crest is directly proportional to the aspect ratio of the dune. Actually, this hydrodynamic property seems to be valid in our model despite rather large dune aspect ratios ($H/L > 0.1$) and the existence of flow separation zones with recirculation eddies above lee sides. Hence, the simple scaling $c \sim 1/H$ between dune height and dune velocity is not valid any more. Instead, the migration speed of a steady state barchan dune has to be inferred from the aspect ratio of the dune as well as from flow velocity and dune height.

[44] Now that we have derived different phenomenological relationships from the outputs of the model, we can use them to quantify different aspects of the mechanics of dunes in nature. For example, we can compare the prediction of our model with some field data gathered by *Elbelrhiti* [2005] on a barchan dune in southwest Morocco. In this region, the mean wind velocity u_* is approximately of 1.7 u_c. The dune is 1.5 m tall and has a length of approximately 25 m in a central cross section parallel to the direction of the wind. The increase in saturated flux from the ground to the crest of the dune is derived from wind velocity measurements. It gives $a \approx 2.75$. Using only the mean wind velocity and the shape of the dune, we can calculate the a value predicted by our model. First, we inject $u_*/u_c = 1.7$ in equation (3) to obtain $Q_{\mathrm{sat}}/Q^0_{\mathrm{sat}} = 0.65$. Then, from the Q_{sat} (τ_1) relationship [see *Narteau et al.*, 2009, Figure 7], we determine the corresponding τ_1 value which is approximately of 8 τ_0. Second, we find $\tau_s^{\mathrm{crest}}/\tau_s^{\mathrm{flat}} \approx 2.6$ by injecting the aspect ratio of the dune in equation (5). Finally, we use Figure 9a to read the a value that corresponds to these specific values of τ_1 and $\tau_s^{\mathrm{crest}}/\tau_s^{\mathrm{flat}}$. Here, we find $a = 2.8$, a value which is in perfect agreement with the field data.

[45] We can repeat the same comparison using the data collected by *Sauermann et al.* [2003] in northeastern Brazil on a much larger dunes: $L = 200$ m, $H = 34$ m, $u_*/u_c = 1.29$, $u_* = 0.36$ ms^{-1}, $q_{\mathrm{sat}}^{\mathrm{crest}} \approx 32 \cdot 10^{-3}$ kg m^{-1} s^{-1} and $a = q_{\mathrm{sat}}^{\mathrm{crest}}/q_{\mathrm{sat}}^{\mathrm{flat}} \approx 4.1$ (note that, as suggested by the authors, we use the relation between the shear velocity and the saturated sand flux proposed by *Sørensen* [1991] to estimate $q_{\mathrm{sat}}^{\mathrm{flat}} = 7.66 \cdot 10^{-3}$ kg m^{-1}s^{-1}). Injected in our model, this dune morphology and this wind velocity correspond to $\tau_s^{\mathrm{crest}}/\tau_s^{\mathrm{flat}} = 3.2$ and $\tau_1 = 14\tau_0$, respectively. In Figure 9a, we read $a = 3.7$, a value which is again in reasonable agreement with observations. Finally, to get a third example and see if there is any tendency in the variation of the a value, we compare the prediction of the model with a barchan dune in Mauritania studied by *Ahmedou et al.* [2007]: $L = 45$ m, $H = 3.4$ m, $u_*/u_c = 1.5$ and $a = q_{\mathrm{sat}}^{\mathrm{crest}}/q_{\mathrm{sat}}^{\mathrm{flat}} \approx 3$. In this case, we obtain $\tau_s^{\mathrm{crest}}/\tau_s^{\mathrm{flat}} = 2.6$, $\tau_1 = 11\tau_0$ and $a = 3.02$, a value which is almost the same as the value inferred from the field data.

[46] From direct measurements of sand flux on the stoss slope of a barchan dune, *Lancaster et al.* [1996] observe that the a value tends to increase with a decreasing flow velocity. Our model (Figure 9a) and the data analyzed in the previous paragraph confirm this observation. In addition, from the best fit of the dune height-velocity relationship in the model, we obtain a H_0 value of approximately 1.7 l_0. For aeolian dune fields in arid desert on Earth and a mean grain diameter of 180 μm, we have $l_0 \approx 0.5$ m [*Narteau et al.*, 2009]. In this case, the H_0 value predicted by the model is consistent with the value of 0.87 m obtained by *Elbelrhiti et al.* [2005] from the dune height-velocity relationship in southwest Morocco. Furthermore, as for this specific set of data, we also find that, in the model, the H_0 values for barchan dunes and superimposed bedforms are the same.

[47] An originality of the model is to produce a hierarchy of dune features (Figure 9c). We show that there is no difference in the morphodynamics of these different generations of dunes, and, because they result from the same instability, we can directly compare the initiation of bedforms on a flat bed with the formation and growth of secondary bedforms on upstream faces of larger dunes. Not surprisingly with respect to what have been learned from primary dunes, the morphodynamics of secondary bedforms may also vary according to flow strength and dune shape. For example,

higher flows produce steeper slopes and superimposed bedforms may be blurred. Hence, large dunes in the model do not always have secondary bedforms (Figure 12). In nature, where flow strength is highly variable over time, a short period of very high flow may therefore limit the occurrence of superimposed bed forms on larger dunes as well. Furthermore, many small to medium sized dunes in the field do not exhibit prominent secondary structures. This is also the case in our model for dunes which have a total length smaller than twice the characteristic length scale $\lambda_{\max}$ for the formation of dune ($\lambda_{\max} \approx 40\ l_0 \approx 20$ m). In fact, in this case, the face exposed to the flow is too small to observe the emergence and growth of a dune pattern.

[48] Our numerical results show that individual barchan dunes are not likely to reach a steady state in dune fields where complex dune-dune interactions and turbulent flow properties produce nonstationary input/output sediment fluxes. We infer that this unstable state should be reinforced in natural dune fields where dunes are permanently subject to change in direction and strength of the flow. Nevertheless, now that we have quantitatively characterized steady state regimes in the model, we can use them to describe transient behaviors in dune fields. Then, we should be able to identify different ingredients that may control the quasi-stationary steady state of barchan dune fields in nature. More generally, because we now understand the role of diffusion, the effect of flow strength and how to limit dune size in the model, we can use it under specific conditions to reproduce specific dunes features in different geophysical environments.

References

Ahmedou, D. O., A. O. Mahfoudh, P. Dupont, A. O. El Moctar, A. Valance, and K. R. Rasmussen (2007), Barchan dune mobility in Mauritania related to dune and interdune sand fluxes, *J. Geophys. Res.*, *112*, F02016, doi:10.1029/2006JF000500.

Andreotti, B., P. Claudin, and S. Douady (2002), Selection of dune shapes and velocities. Part 1: Dynamics of sand, wind and barchans, *Eur. Phys. J. B*, *28*, 321–339.

Andreotti, B., A. Fourrière, F. Ould-Kaddour, B. Murray, and P. Claudin (2009), Size of giant dunes limited by the depth of the atmospheric boundary layer, *Nature*, *457*, 1120–1123, doi:10.1038/nature07787.

Baas, A., and J. Nield (2007), Modelling vegetated dune landscapes, *Geophys. Res. Lett.*, *34*, L06405, doi:10.1029/2006GL029152.

Bagnold, R. A. (1941), *The Physics of Blown Sand and Desert Dunes*, Methuen, London.

Bak, P., C. Tang, and K. Wiesenfield (1988), Self-organised criticality, *Phys. Rev. A*, *38*, 364–374.

Breed, C., and T. Grow (1979), Morphology and distribution of dunes in sand seas observed by remote sensing, in *A Study of Global Sand Seas*, edited by E. McKee, pp. 252–302, U.S. Gov. Print. Off., Washington, D. C.

Bristow, C. S., S. D. Bailey, and N. Lancaster (2000), The sedimentary structure of linear sand dunes, *Nature*, *406*, 56–59.

Charru, F. (2006), Selection of the ripple length on a granular bed, *Phys. Fluids*, *18*, 121508, doi:10.1063/1.2397005.

Chopard, B., and M. Droz (1998), *Cellular automata modeling of physical systems*, Cambridge Univ. Press, Cambridge, U. K.

Claudin, P., and B. Andreotti (2006), A scaling law for aeolian dunes on Mars, Venus, Earth, and for subaqueous ripples, *Earth Planet. Sci. Lett.*, *252*, 30–44.

d'Humières, D., P. Lallemand, and U. Frisch (1986), Lattice gas models for 3D hydrodynamics, *Europhys. Lett.*, *2*, 291–297.

Durán, O., and H. Herrmann (2006), Vegetation against dune mobility, *Phys. Rev. Lett.*, 97.

Elbelrhiti, H. (2005), Morphodynamique des barkhanes: Étude des dunes du sud-ouest marocains, Ph.D. thesis, Univ. Paris VII, Paris.

Elbelrhiti, H., P. Claudin, and B. Andreotti (2005), Field evidence for surface-wave-induced instability of sand dunes, *Nature*, *437*, 720–723.

Elbelrhiti, H., B. Andreotti, and P. Claudin (2008), Barchan dune corridors: Field characterization and investigation of control parameters, *J. Geophys. Res.*, *113*, F02S15, doi:10.1029/2007JF000767.

Ewing, R., G. Kocurek, and L. Lake (2006), Pattern analysis of dune-field parameters, *Earth Surf. Processes Landf.*, *31*, 1176–1191, doi:10.1002/esp.1312.

Finkel, H. J. (1959), The barchans of southern Peru, *J. Geol.*, *67*, 614–647.

Fischer, S., M. E. Cates, and K. Kroy (2008), Dynamic scaling of desert dunes, *Phys. Rev. E*, *77*, 031302.

Frisch, U., B. Hasslacher, and Y. Pomeau (1986), Lattice-gas automata for the Navier-Stokes equation, *Phys. Rev. Lett.*, *56*, 1505–1508.

Groh, C., A. Wierschem, N. Aksel, I. Rehberg, and C. Kruelle (2008), Barchan dunes in two dimensions: Experimental tests for minimal models, *Phys. Rev. E*, *78*, 021304.

Groh, C., I. Rehberg, and C. Kruelle (2009), How attractive is a barchan dune?, *New J. Phys.*, *11*, 023014.

Hastenrath, S. (1967), The barchans of the Arequipa region, southern Peru, *Z. Geomorphol.*, *11*, 300–331.

Hastenrath, S. (1987), The barchan dunes of southern Peru revisited, *Z. Geomorphol.*, *31-2*, 167–178.

Hersen, P. (2004), On the crescentic shape of barchan dunes, *Eur. Phys. J. B*, *37*, 507–514.

Hersen, P., and S. Douady (2005), Collision of barchan dunes as a mechanism of size regulation, *Geophys. Res. Lett.*, *32*, L21403, doi:10.1029/2005GL024179.

Hersen, P., S. Douady, and B. Andreotti (2002), Relevant length scale of barchan dunes, *Phys. Rev. Lett.*, *89*, 264301.

Hersen, P., K. H. Andersen, H. Elbelrhiti, B. Andreotti, P. Claudin, and S. Douady (2004), Corridors of barchan dunes: Stability and size selection, *Phys. Rev. E*, *69*, 011304.

Howard, A., J. Morton, M. Gad El Hak, and D. Pierce (1978), Sand transport model of barchan dune equilibrium, *Sedimentology*, *25*, 307–338.

Jackson, P. S., and J. C. R. Hunt (1975), Turbulent wind flow over a low hill, *Q. J. R. Meteorol. Soc.*, *101*, 929–955.

Kennedy, J. (1963), The mechanics of dunes and antidunes in erodible bed channels, *J. Fluid Mech.*, *16*, 521–544.

Kocurek, G., and R. Ewing (2005), Aeolian dune field self-organization—Implications for the formation of simple versus complex dune-field patterns, *Geomorphology*, *72*, 94–105.

Kroy, K., G. Sauermann, and H. J. Herrmann (2002), Minimal model for aeolian sand dunes, *Phys. Rev. E*, *66*, 031302.

Lancaster, N. (1985), Variations in wind velocity and sand transport on the windward flanks of desert sand dunes, *Sedimentology*, *32*, 581–593.

Lancaster, N. (1992), Relations between dune generations in the Gran Desierto, Mexico, *Sedimentology*, *39*, 631–644.

Lancaster, N. (1995), *Geomorphology of Desert Dunes*, Routledge, New York.

Lancaster, N., W. Nickling, C. Neuman, and V. Wyatt (1996), Sediment flux and airflow on the stoss slope of a barchan dune, *Geomorphology*, *17*, 55–62.

Livingstone, I., and A. Warren (1996), *Aeolian Geomorphology*, Addison-Wesley, Harlow, U. K.

McKee, E. (1979), Introduction to a study of global sand seas, in *A Study of Global Sand Seas*, edited by E. McKee, pp. 3–19, U.S. Gov. Print. Off., Washington, D. C.

Momiji, H., and A. Warren (2000), Relations of sand trapping efficiency and migration speed of transverse dunes to wind velocity, *Earth Surf. Processes Landforms*, *25*, 1069–1084.

Narteau, C., J.-L. Le Mouël, J. Poirier, E. Sepúlveda, and M. G. Shnirman (2001), On a small-scale roughness of the core-mantle boundary, *Phys. Earth Planet. Inter.*, *191*, 49–61.

Narteau, C., D. Zhang, O. Rozier, and P. Claudin (2009), Setting the length and time scales of a cellular automaton dune model from the analysis of superimposed bed forms, *J. Geophys. Res.*, *114*, F03006, doi:10.1029/2008JF001127.

Nishimori, H., and N. Ouchi (1993), Computational models for sand ripple and sand dune formation, *Int. J. Mod. Phys. B*, *7*, 2025–2034.

Nishimori, H., M. Yamasaki, and K. H. Andersen (1999), A simple model for the various pattern dynamics of dunes, *Int. J. Mod. Phys. B*, *12*, 257–272.

Sauermann, G. (2001), Modeling of wind blown sand and desert dunes, Ph.D. thesis, Univ. Stuttgart, Stuttgart, Germany.

Sauermann, G., K. Kroy, and H. J. Herrmann (2001), Continuum saltation model for sand dunes, *Phys. Rev. E*, *64*, 031305.

Sauermann, G., J. S. Andrade, L. P. Maia, U. M. S. Costa, A. D. Araujo, and H. J. Herrmann (2003), Wind velocity and sand transport on a barchan dune, *Geomorphology*, *54*, 245–255.

Schwämmle, V., and H. Herrmann (2005), A model of barchan dunes including lateral shear stress, *Eur. Phys. J. E*, *16*, 57–65, doi:10.1140/epje/e2005-00007-0.

Sørensen, M. (1991), An analytic model of wind-blown sand transport, *Acta Mech.*, 1 suppl., 67–81.

Werner, B. T. (1995), Eolian dunes: Computer simulations and attractor interpretation, *Geology*, *23*, 1107–1110.

Werner, B. T., and D. T. Gillespie (1993), Fundamentally discrete stochastic model for wind ripple dynamics, *Phys. Rev. Lett.*, *71*, 3230–3233.

Werner, B. T., and G. Kocurek (1997), Bed-form dynamics: Does the tail wag the dog?, *Geology*, *25*, 771–774.

Wiggs, G. F. S. (2001), Desert dune processes and dynamics, *Prog. Phys. Geogr.*, *25*, 53–79.

Wiggs, G. F. S., I. Livingstone, and A. Warren (1996), The role of streamline curvature in sand dune dynamics: Evidence from field and wind tunnel measurements, *Geomorphology*, *17*, 29–46.

C. Narteau and D. Zhang, Laboratoire de Dynamique des Fluides Géologiques, Institut de Physique du Globe de Paris, UMR 7154, CNRS, Université Paris 7, 1 Rue Jussieu, Paris, Cedex 05, F-75238, France. (narteau@ipgp.jussieu.fr; dzhang@ipgp.jussieu.fr)

O. Rozier, Service Informatique, Institut de Physique du Globe de Paris, UMR 7154, CNRS, Université Paris 7, 4 Place Jussieu, Paris, Cedex 05, F-75252, France. (rozier@ipgp.jussieu.fr)